

DETC2003/VIB-48426

A SET-VALUED FORCE LAW FOR SPATIAL COULOMB-CONTENSOU FRICTION

Remco I. Leine

Christoph Glocker

Institute of Mechanical Systems,
Center of Mechanics, ETH Zentrum,
CH-8092 Zürich, Switzerland,
remco.leine@imes.mavt.ethz.ch
christoph.glocker@imes.mavt.ethz.ch

ABSTRACT

The aim of this paper is to develop a contact law for combined spatial Coulomb friction and normal friction torque (drilling friction) as a function of sliding velocity and spin. We will call this extended contact law the Coulomb-Contensou friction law and derive it from a non-smooth velocity pseudo potential. A Runge-Kutta time-stepping method is briefly presented for the numerical simulation of rigid bodies with Coulomb-Contensou friction. The algebraic inclusion describing the contact problem is solved with an Augmented Lagrangian approach. The theory and numerical methods are applied to the Tippe-Top, which illustrates the importance of Coulomb-Contensou friction for the dynamics of systems with friction.

INTRODUCTION

Mechanical systems with frictional contact between hard bodies can often well be modelled with a rigid multi-body approach, using set-valued force laws for the constitutive description of the contact. Many practical applications have been successfully studied assuming a set-valued Coulomb friction law together with a restitution law (Glocker, 1995; Leine et al., 2003; Pfeiffer and Glocker, 1996; Stieglmeier, 2001). Fastly spinning spatial objects, however, require a more elaborate friction model which will be studied in this paper.

The set-valued spatial Coulomb friction law describes the friction force $\boldsymbol{\lambda}_T$ of a single contact point with two components $\boldsymbol{\lambda}_T = [\lambda_{T1} \ \lambda_{T2}]^T$. The friction force $\boldsymbol{\lambda}_T$ lies within a disk $\|\boldsymbol{\lambda}_T\| \leq \mu\lambda_N$ on the tangent plane of the contact point, where μ

is the friction coefficient and λ_N is the normal force. The contacting bodies are assumed to be rigid and impenetrable within a rigid multi-body framework and the contact is therefore idealized to be a point. The contact point can not transmit a friction torque and the influence of spin and drilling friction on the sliding friction $\boldsymbol{\lambda}_T$ is therefore usually neglected. In reality, the stiff (but still deformable) bodies deform and touch each other on a small contact surface, being more or less circular. The deformations of stiff bodies are negligible compared to their geometry and the global rigid body motion, but lead to contacting areas which can influence the dynamics of the system. A contact *surface* can not only transmit a sliding force $\boldsymbol{\lambda}_T$, but also a friction torque τ_N normal to the contact surface. The effective radius of the contact surface is influenced by the normal contact force λ_N , the elasticity of the contacting bodies, the surface roughness and the pressure distribution. The friction torque is in most applications neglected because the effective radius is very small in practice. If, however, an object is spinning fastly, then the influence of spin and drilling friction on the dynamics becomes large and can no longer be neglected.

Contensou (1963) realized that drilling friction and spin are important for the dynamics of fastly spinning tops. A fastly spinning top experiences very little resistance in sliding direction and easily wanders over the floor. The same phenomenon occurs in an electric polishing machine with turning brushes used to clean floors (Magnus, 1971). The machine is hard to move when the brushes are non-rotating but the machine can easily be pushed over the floor with rotating brushes. Contensou calculated the dependence of the sliding friction force on the slid-

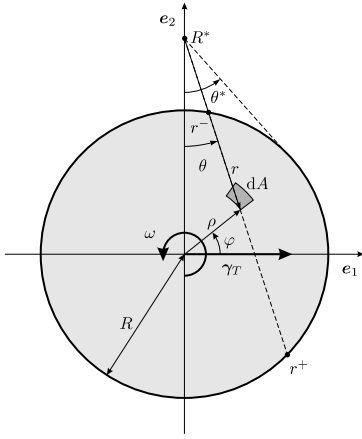


Figure 1. Coordinates at the contact surface.

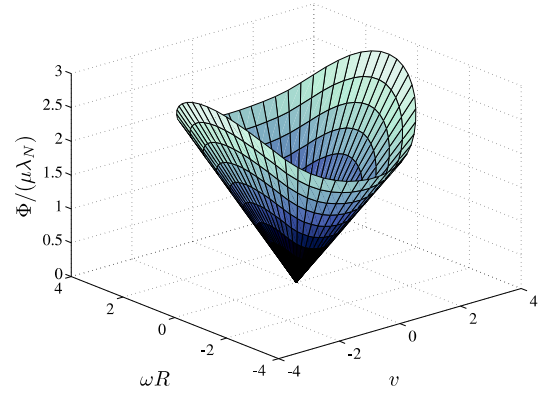


Figure 2. The velocity potential Φ as function of v and ωR .

ing velocity v and spin ω , and showed that the sliding friction force vanishes when the ratio $\frac{v}{\omega R}$ tends to zero. Magnus (1971) used Contensou's friction law to study the stability of the Tippe-Top. Contensou (1963) expressed the friction force in elliptic integrals, which Zhuravlev (1998) transformed for a parabolic pressure distribution into elementary functions using other coordinates. The elliptic integrals can not be simplified to elementary functions if a uniform pressure distribution is assumed.

We will formulate Contensou's spatial friction law in the framework of potential theory and subdifferentials, much like the treatment of spatial Coulomb friction in (Glocker, 2001). The friction force and friction torque, as a function of sliding velocity and spin, will be derived by taking the subdifferential of a velocity pseudo potential. The dependence of the maximal friction torque on the friction force (and vice versa) will be studied during sticking (no sliding + no spin). A time-stepping method, based on an Augmented Lagrangian approach, will be presented for the numerical time-integration of systems with Coulomb-Contensou friction. Finally, the theory and numerical methods are applied to the Tippe-Top, which illustrates the importance of Coulomb-Contensou friction for the dynamics of systems with friction.

UNIFORM PRESSURE DISTRIBUTION

Friction force and torque are influenced by the pressure distribution over the contact surface, which depends on the geometry and elasticity properties of the contacting bodies. Local deformations are not modelled within a rigid multi-body approach. A pressure distribution has to be assumed or to be estimated with analytical methods from the undeformed geometry of the contacting bodies. The pressure distribution can often well be modelled by a parabolic or a uniform distribution, depending on the geometry of the contacting bodies. A set-valued contact law for a uniform pressure distribution will be derived in this section and

for a parabolic pressure distribution in the next section.

The contact surface (Figure 1) is assumed to be circular with radius R . The relative sliding velocity of the contact is denoted by $\boldsymbol{\gamma}_T$ and the spin by $\boldsymbol{\omega}$. We introduce an orthonormal coordinate frame $(\mathbf{e}_1, \mathbf{e}_2, \mathbf{e}_3)$, of which \mathbf{e}_1 and \mathbf{e}_2 span the contact tangent plane. Without loss of generality we assume that $\boldsymbol{\gamma}_T = v\mathbf{e}_1$. The sliding velocity is expressed by the scalar value v . The spin $\boldsymbol{\omega}$ is normal to the contact plane $\boldsymbol{\omega} = \omega\mathbf{e}_3$. A surface element dA , with polar coordinates (ρ, φ) , has a sliding velocity of $\mathbf{w} = (v - \omega\rho \sin \varphi)\mathbf{e}_1 + (\omega\rho \cos \varphi)\mathbf{e}_2$. A normal force σdA is acting at the surface element. The normal contact force between the contacting bodies is $\lambda_N = \iint \sigma dA$.

We will derive a velocity pseudo potential, which serves as a dissipation function. The velocity *pseudo* potential is dependent on the normal contact force, which is in turn dependent on the motion of the system and is therefore not a true potential. The word 'pseudo' will be omitted for brevity. Coulomb's law is assumed to hold on an arbitrary surface element dA with sliding velocity \mathbf{w} . The magnitude of the friction force on dA is $d\boldsymbol{\lambda}_T = \mu\sigma dA \frac{\mathbf{w}}{\|\mathbf{w}\|}$ yielding a velocity potential $d\Phi = \mathbf{w}^T d\boldsymbol{\lambda}_T = \mu\sigma\|\mathbf{w}\| dA$. The velocity potential for the total contact surface is obtained by integrating over the contact surface

$$\Phi(\mathbf{w}, \sigma) = \iint_A \mu\sigma\|\mathbf{w}\| dA. \quad (1)$$

Substituting the normal stress for a uniform pressure distribution $\sigma = \frac{\lambda_N}{A}$ in (1) and making use of the coordinate system (ρ, φ) gives the double integral

$$\Phi(v, \omega, \lambda_N) = \frac{\mu\lambda_N}{\pi R^2} \int_0^R \int_0^{2\pi} \rho \sqrt{v^2 + (\omega\rho)^2 - 2\omega\rho v \sin \varphi} d\varphi d\rho. \quad (2)$$

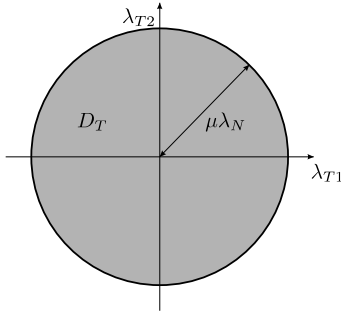


Figure 3. Friction disk; admissible forces for $\lambda_\tau = 0$.

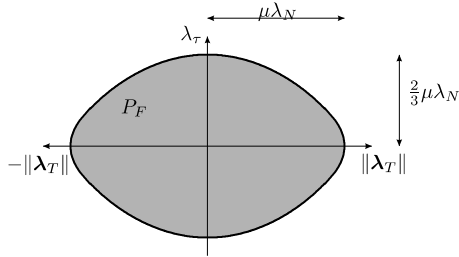


Figure 4. Friction plate; admissible force and torque.

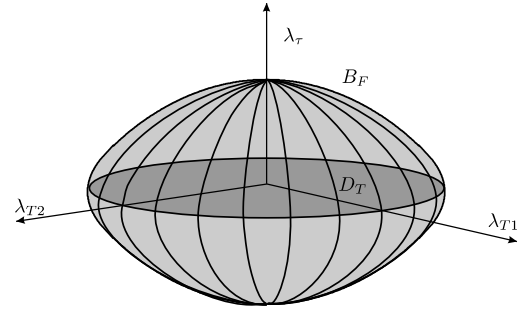


Figure 5. Friction ball B_F .

Note that the velocity potential is a smooth function of $|v|$ and $|\omega|$. The force laws are set-valued at $(v, \omega R) = \mathbf{0}$.

The classical Coulomb's friction law for spatial contact, without spin and friction torque, states that the set of admissible tangential contact forces is the convex set $D_T := \{\lambda_T \mid \|\lambda_T\| \leq \mu\lambda_N\}$, where $D_T(\lambda_N)$ is addressed as the *friction disk* and is a function of the normal force λ_N (Figure 3). The tangential contact law is for pure Coulomb friction given by

$$-\gamma_T \in N_{D_T}(\lambda_T), \quad (5)$$

where $N_{D_T}(\lambda_T)$ is the normal cone to D_T at λ_T . The friction torque τ_N is normalized to a force $\lambda_\tau = \frac{\tau_N}{R}$ and the angular spin velocity ω to a velocity $\gamma_\tau = \omega R$. We now extend the existing theory for spatial Coulomb friction to spatial Coulomb-Contensou friction taking into account a nonzero friction torque τ_N . The force laws (4) give the values of λ_T and λ_τ as a function of γ_T and γ_τ and implicitly define the set of admissible values of λ_T and λ_τ . The admissible set of $(\|\lambda_T\|, \lambda_\tau)$ is called the *friction plate* P_F (Figure 4). The admissible set of tangential friction forces and normal friction torque forms a squashed ball $B_F(\lambda_N)$ in the $(\lambda_{T1}, \lambda_{T2}, \lambda_\tau)$ space. The *friction ball* B_F (Figure 5), is axisymmetric around the λ_τ axis. The intersection of B_F with the $(\lambda_{T1}, \lambda_{T2})$ plane is formed by the friction disk D_T . Any intersection of B_F orthogonal to D_T will give the friction plate P_F . The contact law for spatial Coulomb-Contensou friction can now be expressed by means of the friction ball B_F

$$-\gamma_F \in N_{B_F}(\lambda_F), \quad (6)$$

with $\gamma_F^T = [\gamma_{T1} \ \gamma_{T2} \ \gamma_\tau]$ and $\lambda_F^T = [\lambda_{T1} \ \lambda_{T2} \ \lambda_\tau]$ where $N_{B_F}(\lambda_F)$ is the normal cone to $B_F(\lambda_N)$ at λ_F .

The magnitudes of λ_T and λ_τ as a function of u and $1/u$ are shown in Figures 6 and 7 (solid lines). The functions both start at the origin and have an asymptote at $\|\lambda_T\| = \mu\lambda_N$ and $|\lambda_\tau| = \frac{2}{3}\mu\lambda_N$ respectively. The friction characteristic $\lambda_T(v)$ for a fixed value of γ_τ can be derived from (4) and is shown in Figure 8 for different fixed values of γ_τ . The curves for $\gamma_\tau > 0$ are all

The double integral (2) can be approximated with Taylor series which results in the velocity potential Φ

$$\Phi(v, \omega, \lambda_N) = \begin{cases} \mu\lambda_N|\omega|R\left(\frac{2}{3} + \frac{1}{2}u^2 - \frac{1}{32}u^4 - \frac{1}{384}u^6 + O(u^8)\right), & u \leq 1 \\ \mu\lambda_N|\omega|R\left(u + \frac{1}{8}\frac{1}{u} + \frac{1}{192}\frac{1}{u^3} + \frac{1}{1024}\frac{1}{u^5} + O\left(\frac{1}{u^7}\right)\right), & u > 1 \end{cases} \quad (3)$$

where $u = \frac{|v|}{|\omega|R} = \frac{R^*}{R}$ and $R^* = \frac{|v|}{|\omega|}$. Apparently, the velocity potentials for the purely sliding and purely rotating case are

$$\Phi_{\omega=0} = \mu\lambda_N|v| = \mu\lambda_N\|\gamma_T\|, \quad \Phi_{v=0} = \frac{2}{3}\mu\lambda_N|\omega|R,$$

which are non-smooth convex potentials. The velocity potential Φ forms a cone as function of v and ωR (Figure 2). The contour lines of the cone are a form between an ellipse and a rectangle.

The tangential friction λ_T and the friction torque τ_N can be derived from the velocity potential (3) (Glocker, 2001) via the subdifferential

$$-\lambda_T \in \partial_{\gamma_T} \Phi, \quad -\tau_N \in \partial_{\omega} \Phi, \quad (4)$$

or, by the chain rule

$$-\lambda_T \in \partial_{\gamma_T} \|\gamma_T\| \nabla_{|v|} \Phi, \quad -\tau_N \in \partial_{\omega} |\omega| \nabla_{|\omega|} \Phi.$$

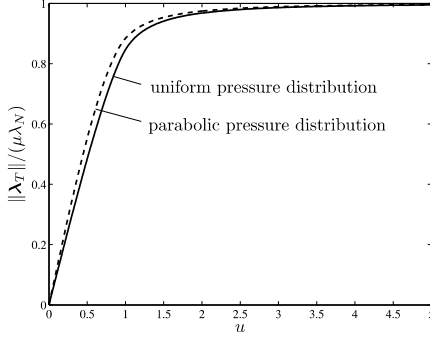


Figure 6. Friction force as a function of u for a uniform pressure distribution (solid) and for a parabolic pressure distribution (dashed).

single-valued functions of v . Apparently, a superimposed spin ω on a sliding velocity v causes a smoothing effect of the friction characteristic $\lambda_T(v)$. The friction characteristic for $\gamma_\tau = 0$ is (for $\lambda_\tau = 0$) the classical set-valued friction characteristic of Coulomb. Similarly, the dependence of λ_τ on γ_τ , for different fixed values of v , is shown in Figure 9. The same smoothing effect occurs in the $\lambda_\tau(\gamma_\tau)$ relationship due to a superimposed velocity $v > 0$. Again, a set-valued relationship is obtained for $v = 0$. The boundaries $\|\lambda_T\| = \mu\lambda_N$ and $|\lambda_\tau| = \frac{2}{3}\mu\lambda_N$ of the sets for $v = \gamma_\tau = 0$ are the extreme values of the friction ball $B_F(\lambda_N)$ along its principal axes. For the classical set-valued friction characteristic of Coulomb, the magnitude friction force $\|\lambda_T\|$ rises up to the value $\mu\lambda_N$ when the contact changes from a sticking state to sliding. This is in general *not* the case for Coulomb-Contensou friction as soon as we have some rotation. The slip-criterion for Coulomb-Contensou friction is given by $(\lambda_T, \lambda_\tau) \in \text{bdry } B_F(\lambda_N)$.

PARABOLIC PRESSURE DISTRIBUTION

In the previous section we studied a contact with uniform pressure distribution by means of Taylor series. The velocity potential with a parabolic pressure distribution, however, can be expressed in elementary functions (Zhuravlev, 1998) using polar coordinates r and θ around the pole $R^*\mathbf{e}_2$ (Figure 1). The relation between the coordinates (r, θ) and (ρ, φ) is given by $\rho \cos \varphi = r \sin \theta$ and $\rho \sin \varphi + r \cos \theta = R^* = |\frac{v}{\omega}|$. We will assume a circular contact surface with radius R , which is for a Hertz contact (Johnson, 1985) a function of the normal load λ_N . However, the theoretical contact radius according to Hertz is for relatively hard bodies extremely small. Instead, we will assume that the radius of the contact surface is determined by the surface roughness and meso-scopic non-convexity of the contacting bodies, which is for hard bodies more realistic. The contact radius is therefore assumed to be constant. The Hertz pressure distribution is given by the parabolic function $\sigma = \frac{3\lambda_N}{2\pi R^2} \sqrt{1 - \frac{\rho^2}{R^2}}$. The integral (1) can

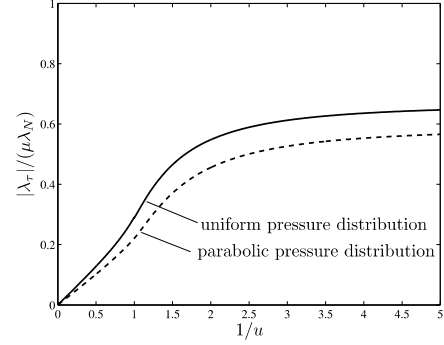


Figure 7. Friction torque as a function of u for a uniform pressure distribution (solid) and for a parabolic pressure distribution (dashed).

be evaluated in the coordinates (r, θ) and the velocity potential for a parabolic pressure distribution can be obtained

$$\Phi(v, \omega, \lambda_N) = \begin{cases} \frac{3\mu\lambda_N}{128} R |\omega| \pi (-u^4 + 8u^2 + 8), & u \leq 1, \\ \frac{3\mu\lambda_N}{64} R |\omega| \left((-u^4 + 8u^2 + 8) \arcsin \frac{1}{u} + (u^2 + 14) \sqrt{u^2 - 1} \right), & u > 1, \end{cases} \quad (7)$$

where $u = u(v, \omega)$ and R is constant.

The set-valued force laws for Coulomb-Contensou friction with a parabolic pressure distribution can be derived from the velocity potential (7) similar to the discussion of the uniform pressure distribution. The magnitude of the friction force λ_T as a function of u and $\lambda_\tau = \frac{\omega v}{R}$ as a function of $1/u$ for a parabolic pressure distribution is shown in Figures 6 and 7 (dashed lines). Similar to the discussion of the uniform pressure distribution, one can express the contact law for spatial Coulomb-Contensou friction with parabolic pressure distribution by means of the friction ball B_F . The force laws for a parabolic pressure distribution are qualitatively similar to the force laws for a uniform pressure distribution and differ maximally about 20 percent in magnitude (see Figures 6 and 7). The friction plate P_F and friction ball B_F for a parabolic pressure distribution (not depicted) are therefore very similar in shape to the sets shown in Figures 4 and 5.

MULTI-BODY FORMULATION OF SYSTEMS WITH COULOMB-CONTENSOU FRICTION

The main rigid-body integration techniques for systems with unilateral constraints are the event-driven integration method and the time-stepping method (Anitescu and Potra, 1997; Brogliato, 1999; Glocker, 1995, 1998; Moreau, 1988; Pfeiffer and Glocker, 1996; Stiegemeyer, 2001). Time-stepping methods are based on using a time-discretization of generalized positions \mathbf{q} and velocities \mathbf{u} , usually with a fixed step-size. Integrals of forces over

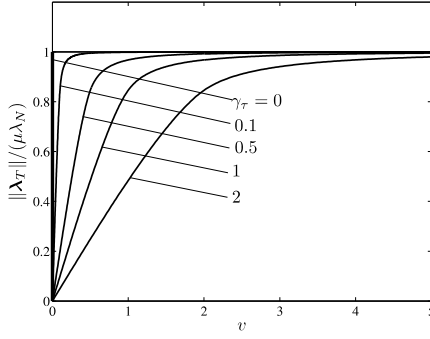


Figure 8. Dependence of friction force on γ_τ and v for a uniform pressure distribution.

each time-step are used instead of the instantaneous values of the forces. The time-stepping method makes no distinction between impulsive forces (due to impacts) and finite forces. Only increments of the positions and velocities are computed. The acceleration $\dot{\mathbf{u}}$ is not computed by the algorithm, as it becomes infinite for impulsive forces. The positions and velocities at the end of the time-step are found by solving an algebraic inclusion which describes the contact problem (for instance by formulating it as a (Non)linear Complementarity Problem). Multiple events might take place during one time-step, and the algorithm computes the overall integral of the forces over this time-step, which is finite. The time-stepping method is especially useful when one is interested in the global motion of systems with many contact points, leading to a large number of events. Each individual event is for those applications not of importance but the global motion is determined by the sum of all events. The time-stepping method was introduced by Moreau (1988) and has been subsequently developed in (Anitescu and Potra, 1997; Stiegelmeier, 2001).

The time-stepping method and the event-driven integration method have been applied to mechanical systems with *Coulomb* friction. In this section we will describe the time-stepping method of Moreau (1988) and combine it with the Augmented Lagrangian Method (Alart and Curnier, 1991) in order to solve the *Coulomb-Contensou* contact problem. Furthermore, we will extend the time-stepping method of Moreau to a Runge-Kutta time-stepping method. A brief discussion of the Augmented Lagrangian will be given first.

The dynamics of a multi-body system during an impact free part of the motion can be expressed by the equation of motion on acceleration level (Pfeiffer and Glocker, 1996)

$$\mathbf{M}(t, \mathbf{q}) \dot{\mathbf{u}} - \mathbf{h}(t, \mathbf{q}, \dot{\mathbf{q}}) - \mathbf{W}_N(t, \mathbf{q}) \boldsymbol{\lambda}_N - \mathbf{W}_F(t, \mathbf{q}) \boldsymbol{\lambda}_F = \mathbf{0}, \quad (8)$$

with the set-valued force laws

$$-\mathbf{g}_N \in N_{C_N}(\boldsymbol{\lambda}_N), \quad -\boldsymbol{\gamma}_F \in N_{B_F(\boldsymbol{\lambda}_N)}(\boldsymbol{\lambda}_F), \quad (9)$$

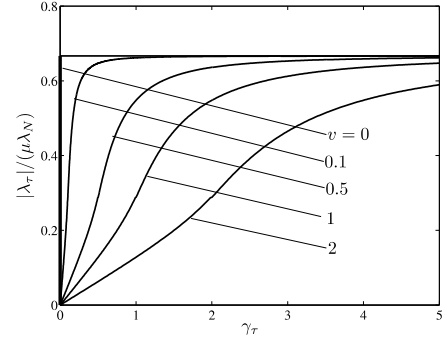


Figure 9. Dependence of normalized torque on γ_τ and v for a uniform pressure distribution.

where \mathbf{M} is the symmetric mass matrix, \mathbf{q} the vector with generalized coordinates, $\mathbf{u} = \dot{\mathbf{q}}$ is the vector with generalized velocities and \mathbf{h} is the vector with all smooth elastic, gyroscopic and dissipating generalized forces. The normal contact force of contact i is denoted by λ_{Ni} and the vector of generalized friction forces by $\boldsymbol{\lambda}_{Fi}$. The vectors \mathbf{w}_{Ni} and \mathbf{w}_{Fi} are the generalized normal and sliding force directions of contact i and constitute the matrices $\mathbf{W}_N = \{\mathbf{w}_{Ni}\}$ and $\mathbf{W}_F = \{\mathbf{w}_{Fi}\}$. The dual variables to the normal contact forces $\boldsymbol{\lambda}_N$ are the variations of the contact distances \mathbf{g}_N and the dual variables to the generalized friction forces $\boldsymbol{\lambda}_F$ are the variations of the generalized sliding velocities $\boldsymbol{\gamma}_F$.

The usual equation of motion, which relates acceleration to forces, is not suited to describe motion with impact. We replace the equation of motion on acceleration level by an equality of measures (Glocker, 2001; Moreau, 1988)

$$\mathbf{M} d\mathbf{u} - \mathbf{h} dt - \mathbf{W}_N d\boldsymbol{\Lambda}_N - \mathbf{W}_F d\boldsymbol{\Lambda}_F = \mathbf{0}, \quad (10)$$

where the dependence on t, \mathbf{q} and $\dot{\mathbf{q}}$ has been omitted for brevity. We denote with dt the Lebesgue-measure and with $d\eta$ the sum of the dirac pulses at the impact times. The measure for the velocities $d\mathbf{u} = \dot{\mathbf{u}} dt + (\mathbf{u}^+ - \mathbf{u}^-) d\eta$ is split in a Lebesgue-measurable part and an atomic part. The atomic part consists of the left and right limit of \mathbf{u} at t . For impact free motion it holds that $d\mathbf{u} = \dot{\mathbf{u}} dt$. Similarly, the measure for the impulses is defined as $d\boldsymbol{\Lambda} = \boldsymbol{\lambda} dt + \boldsymbol{\Lambda} d\eta$. The constraints on velocity level can be expressed in the left and right limits of \mathbf{u} , i.e. $\boldsymbol{\gamma}^+ = \mathbf{W}^T \mathbf{u}^+ + \tilde{\mathbf{w}}$ and $\boldsymbol{\gamma}^- = \mathbf{W}^T \mathbf{u}^- + \tilde{\mathbf{w}}$ with $\boldsymbol{\gamma} = \boldsymbol{\gamma}^+ = \boldsymbol{\gamma}^-$ for impact free motion.

The measure differential equation is discretized by integrating over a small but finite time interval Δt

$$\int_{\Delta t} d\mathbf{u} = \Delta \mathbf{u}, \quad \int_{\Delta t} \mathbf{h} dt = \Delta \mathbf{h} \approx \mathbf{h} \Delta t, \quad \int_{\Delta t} d\boldsymbol{\Lambda} = \boldsymbol{\Lambda},$$

and we obtain the equation of motion in differences

$$\mathbf{M}\Delta\mathbf{u} - \mathbf{h}\Delta t - \mathbf{W}_N\boldsymbol{\Lambda}_N - \mathbf{W}_F\boldsymbol{\Lambda}_F = \mathbf{0}. \quad (11)$$

The force laws for completely inelastic contact with friction can be put in the form

$$-\boldsymbol{\Lambda}_N \in \partial\Psi_{\mathbb{R}^+}(\boldsymbol{\gamma}_N^+), \quad -\boldsymbol{\Lambda}_F \in \partial\Phi(\boldsymbol{\gamma}_F^+), \quad (12)$$

where $\Psi_{\mathbb{R}^+}$ is the indicator function of convex analysis on \mathbb{R}^+ with $\boldsymbol{\gamma}_N^+ = \mathbf{W}_N^T(\mathbf{u}^- + \Delta\mathbf{u}) + \tilde{\mathbf{w}}_N$ and $\boldsymbol{\gamma}_F^+ = \mathbf{W}_F^T(\mathbf{u}^- + \Delta\mathbf{u}) + \tilde{\mathbf{w}}_F$.

In each incremental step, say time-step, we have to solve $\Delta\mathbf{u}$ and $(\boldsymbol{\Lambda}_N, \boldsymbol{\Lambda}_F)$ from the equation of motion (11) and the force laws (12), which forms a set of algebraic *inclusions*. An elegant way to solve such a set of algebraic inclusions is by transforming the problem to a constrained optimization problem. The constrained optimization problem can subsequently be transformed to an *unconstrained* mini-max problem by making use of the Augmented Lagrangian (Rockafellar, 1976). The solution to the algebraic inclusion then corresponds to a saddle-point of the Augmented Lagrangian.

The (quasi) Augmented Lagrangian for a frictional contact problem can be expressed as (Alart and Curnier, 1991)

$$\begin{aligned} L_A(\Delta\mathbf{u}, \boldsymbol{\Lambda}_N, \boldsymbol{\Lambda}_F) &= \frac{1}{2}\|\Delta\mathbf{u} - \mathbf{M}^{-1}\mathbf{h}\Delta t\|_{\mathbf{M}}^2 \\ &\quad - \boldsymbol{\gamma}_N^T(\Delta\mathbf{u})\boldsymbol{\Lambda}_N + \frac{r}{2}\|\boldsymbol{\gamma}_N(\Delta\mathbf{u})\|^2 - \frac{1}{2r}\text{dist}_{C_N}^2(\boldsymbol{\Lambda}_N - r\boldsymbol{\gamma}_N(\Delta\mathbf{u})) \\ &\quad - \boldsymbol{\gamma}_F^T(\Delta\mathbf{u})\boldsymbol{\Lambda}_F + \frac{r}{2}\|\boldsymbol{\gamma}_F(\Delta\mathbf{u})\|^2 - \frac{1}{2r}\text{dist}_{B_F}^2(\boldsymbol{\Lambda}_F - r\boldsymbol{\gamma}_F(\Delta\mathbf{u})), \end{aligned}$$

where B_F is dependent on the normal force¹ and $r > 0$. The value of r should be taken large enough to make the problem well conditioned in the constrained region, but not too large in order to prevent ill-conditioning due to the penalty term $\frac{r}{2}\|\boldsymbol{\gamma}(\Delta\mathbf{u})\|^2$.

We will make use of the following properties of distances and proximal points on a convex set C

$$\text{prox}_C(\mathbf{x}) = \underset{\forall \mathbf{x}^* \in C}{\text{argmin}} \|\mathbf{x} - \mathbf{x}^*\|, \quad \text{dist}_C(\mathbf{x}) = \|\mathbf{x} - \text{prox}_C(\mathbf{x})\|, \quad (13)$$

$$\nabla \frac{1}{2}\text{dist}_C^2(\mathbf{x}) = \mathbf{x} - \text{prox}_C(\mathbf{x}), \quad (14)$$

$$\begin{aligned} f(\mathbf{x}) &= -\mathbf{x}^T\mathbf{y} + \frac{1}{2}\|\mathbf{x}\|^2 - \frac{1}{2}\text{dist}_C^2(\mathbf{y} - \mathbf{x}) \\ \implies \nabla f(\mathbf{x}) &= -\mathbf{y} + \mathbf{x} + [\mathbf{y} - \mathbf{x} - \text{prox}_C(\mathbf{y} - \mathbf{x})] = -\text{prox}_C(\mathbf{y} - \mathbf{x}). \end{aligned} \quad (15)$$

¹To be more precise $B_F = B_F(\text{prox}_{\mathbb{R}^+}(\boldsymbol{\Lambda}_N - r\boldsymbol{\gamma}_N(\Delta\mathbf{u})))$ (Alart and Curnier, 1991).

Evaluating the stationarity conditions of the saddle-point of L_A gives the equations

$$\begin{aligned} \nabla_{\Delta\mathbf{u}}L_A(\Delta\mathbf{u}, \boldsymbol{\Lambda}_N, \boldsymbol{\Lambda}_F) &= \mathbf{M}\Delta\mathbf{u} - \mathbf{h}\Delta t \\ &\quad - \mathbf{W}_N\Pi_N(\boldsymbol{\Lambda}_N, \boldsymbol{\gamma}_N) - \mathbf{W}_F\Pi_F(\boldsymbol{\Lambda}_N, \boldsymbol{\Lambda}_F, \boldsymbol{\gamma}_F) = \mathbf{0} \\ \nabla_{\boldsymbol{\Lambda}_N}L_A(\Delta\mathbf{u}, \boldsymbol{\Lambda}_N, \boldsymbol{\Lambda}_F) &= -\frac{1}{r}(\boldsymbol{\Lambda}_N - \Pi_N(\boldsymbol{\Lambda}_N, \boldsymbol{\gamma}_N)) = \mathbf{0} \\ \nabla_{\boldsymbol{\Lambda}_F}L_A(\Delta\mathbf{u}, \boldsymbol{\Lambda}_N, \boldsymbol{\Lambda}_F) &= -\frac{1}{r}(\boldsymbol{\Lambda}_F - \Pi_F(\boldsymbol{\Lambda}_N, \boldsymbol{\Lambda}_F, \boldsymbol{\gamma}_F)) = \mathbf{0}, \end{aligned} \quad (16)$$

where use has been made of (13) – (15) and the abbreviations

$$\begin{aligned} \Pi_N(\boldsymbol{\Lambda}_N, \boldsymbol{\gamma}_N) &= \text{prox}_{C_N}(\boldsymbol{\Lambda}_N - r\boldsymbol{\gamma}_N), \\ \Pi_F(\boldsymbol{\Lambda}_N, \boldsymbol{\Lambda}_F, \boldsymbol{\gamma}_F) &= \text{prox}_{B_F(\boldsymbol{\Lambda}_N)}(\boldsymbol{\Lambda}_F - r\boldsymbol{\gamma}_F). \end{aligned}$$

Note that $\boldsymbol{\gamma}_N = \boldsymbol{\gamma}_N(\Delta\mathbf{u})$ and $\boldsymbol{\gamma}_F = \boldsymbol{\gamma}_F(\Delta\mathbf{u})$. We therefore obtain the set of algebraic equations

$$\begin{aligned} \mathbf{M}\Delta\mathbf{u} - \mathbf{h}\Delta t - \mathbf{W}_N\Pi_N(\boldsymbol{\Lambda}_N, \boldsymbol{\gamma}_N) - \mathbf{W}_F\Pi_F(\boldsymbol{\Lambda}_N, \boldsymbol{\Lambda}_F, \boldsymbol{\gamma}_F) &= \mathbf{0}, \\ \boldsymbol{\Lambda}_N &= \Pi_N(\boldsymbol{\Lambda}_N, \boldsymbol{\gamma}_N), \\ \boldsymbol{\Lambda}_F &= \Pi_F(\boldsymbol{\Lambda}_N, \boldsymbol{\Lambda}_F, \boldsymbol{\gamma}_F). \end{aligned}$$

The saddle point of the Augmented Lagrangian, being the solution to the set of algebraic equations, can for instance be found with a Modified Newton algorithm (Alart and Curnier, 1991).

We will present a time-stepping method, which uses the Augmented Lagrangian Method to solve the contact problem. Consider the positions \mathbf{q}_A and velocities \mathbf{u}_A known at the beginning of the time-step at time t_A . The algorithm takes first a half time-step for the positions and arrives at the midpoint $\mathbf{q}_M = \mathbf{q}_A + \frac{1}{2}\Delta t\mathbf{u}_A$. The midpoint is used to classify the status of the normal constraints, which allows for an index reduction. The contact set $I_N = \{i \mid g_{Ni}(t_M, \mathbf{q}_M) \leq 0\}$ is calculated at the midpoint and used to set-up the contact problem on velocity level for both the normal and tangential constraints. The set I_N contains all indices of the closed contact points. The velocity \mathbf{u}_E , at the end of time-step $t_E = t_A + \Delta t$, is subsequently calculated by a trapezoidal scheme

$$\mathbf{M}_M(\mathbf{u}_E - \mathbf{u}_A) = \mathbf{h}_M\Delta t + \mathbf{W}_{NM}\boldsymbol{\Lambda}_N + \mathbf{W}_{FM}\boldsymbol{\Lambda}_F,$$

and the set-valued force laws

$$-\boldsymbol{\Lambda}_N \in \partial\Psi_{\mathbb{R}^+}(\boldsymbol{\gamma}_N^+), \quad -\boldsymbol{\Lambda}_F \in \partial\Phi(\boldsymbol{\gamma}_F^+),$$

where \mathbf{M}_M , \mathbf{h}_M , \mathbf{W}_{NM} and \mathbf{W}_{FM} are the system matrices evaluated at the midpoint. This set of algebraic inclusions can be solved using an Augmented Lagrangian approach together with a Modified Newton Method. Finally, the positions at the end of the time-step are calculated $\mathbf{q}_E = \mathbf{q}_M + \frac{1}{2}\Delta t\mathbf{u}_E$.

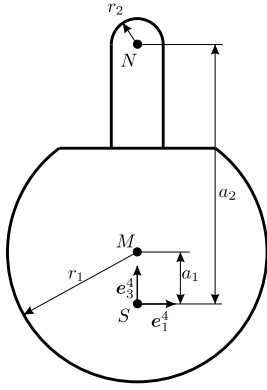


Figure 10. Geometry of the Tipped-Top.

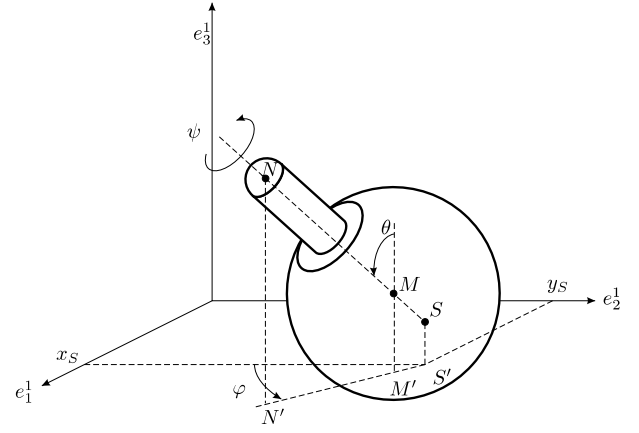


Figure 11. The Euler angles of the Tipped-Top.

The time-stepping method of Moreau (1988) is very elegant due to its simplicity but is at best a second-order method. High frequency oscillations during smooth parts of the motion require a higher-order integration scheme. A Runge-Kutta integration method for ordinary differential equations can be adapted to measure differential equations. For a mechanical system with impacts, one cannot determine accelerations nor contact forces because they are not functions of bounded variation if an impact occurs. Still, for a discretized measure differential equation we are able to define an average acceleration per time-step $\mathbf{a}^j = (\mathbf{u}^j - \mathbf{u}^{j-1})/\Delta t$, which will be denoted by ‘pseudo-acceleration’. The average acceleration, taking into account the set-valued behaviour of the contact forces, can be computed with the method of Moreau. A Runge-Kutta method for systems with impact and friction can therefore be formulated, which uses the time-stepping method of Moreau to compute pseudo-accelerations at every stage of the Runge-Kutta scheme.

THE TIPPE-TOP

We will present a rigid-body model of the Tipped-Top and numerical results using a Runge-Kutta time-stepping method and Coulomb-Contensou’s friction law. The Tipped-Top (Figure 10) consists of a spherical body with geometric center M , radius r_1 , and a stick attached on top of the body. The stick is rounded at the tip with a hemisphere with geometric center N and radius r_2 . The toy is axisymmetric around the axis MN . The center of mass of the top is the point S at a distance a_1 below M and at a distance a_2 from N .

The $\mathbf{e}^1 = [\mathbf{e}_1^1, \mathbf{e}_2^1, \mathbf{e}_3^1]^T$ coordinate frame is the orthonormal absolute coordinate frame fixed to the world where \mathbf{e}_3^1 points in the vertical direction. The frame $\mathbf{e}^4 = [\mathbf{e}_1^4, \mathbf{e}_2^4, \mathbf{e}_3^4]^T$ is fixed to the body with \mathbf{e}_3^4 along the axis of symmetry. The rotation of the top will be described in standard Euler angles θ (nutation), φ (precession) and ψ (spin angle) (Figure 11). As generalized coordi-

ates for the top we choose the positions x_S, y_S and z_S along the axes $\mathbf{e}_1^1, \mathbf{e}_2^1, \mathbf{e}_3^1$ to describe the translational motion of the center of mass S and the Euler angles θ, φ and ψ to describe the rotational motion, i.e. $\mathbf{q} = [x_S, y_S, z_S, \theta, \varphi, \psi]^T$. The kinetic energy T can be expressed in the generalized coordinates

$$\begin{aligned} T &= \frac{1}{2}m(\dot{x}_S^2 + \dot{y}_S^2 + \dot{z}_S^2) + \frac{1}{2}I_1(\dot{\omega}_1^4)^2 + \frac{1}{2}I_2(\dot{\omega}_2^4)^2 + \frac{1}{2}I_3(\dot{\omega}_3^4)^2 \\ &= \frac{1}{2}m(\dot{x}_S^2 + \dot{y}_S^2 + \dot{z}_S^2) + \frac{1}{2}I_1(\dot{\varphi}^2 \sin^2 \theta + \dot{\theta}^2) + \frac{1}{2}I_3(\dot{\psi} + \dot{\varphi} \cos \theta)^2, \end{aligned}$$

with $I_1 = I_2$ due to axisymmetry. The potential energy V is purely due to gravity, $V = mgz_S$. The Lagrange’s equation of motion for the unconstrained undamped motion is $\frac{d}{dt}T_{,\dot{q}} - T_{,q} + V_{,q} = 0$. The equations of motion can be put in the form $\mathbf{M}(\mathbf{q})\ddot{\mathbf{q}} - \mathbf{h}(\mathbf{q}, \dot{\mathbf{q}}) = \mathbf{0}$, where \mathbf{M} is the mass matrix and \mathbf{h} is a vector containing gyroscopical and gravitational forces.

The top has two contact points (either open or closed). Contact point 1 is the contact between the body and the floor. Contact point 2 is the contact between the tip of the stick and the floor. The point on the spherical part of the top, being closest to the projection point M' , is called point C . Contact is established when C agrees with M' and then we call C the contact point with location

$$\mathbf{r}_C = \begin{bmatrix} x_S + a_1 \sin \varphi \sin \theta \\ y_S - a_1 \cos \varphi \sin \theta \\ z_S + a_1 \cos \theta - r_1 \end{bmatrix},$$

The third component of \mathbf{r}_C is the contact distance of contact 1

$$g_{N1} = z_S + a_1 \cos \theta - r_1.$$

Similarly, the contact distance between the stick and the floor reads as $g_{N2} = z_S + a_2 \cos \theta - r_2$. The contact distances have the

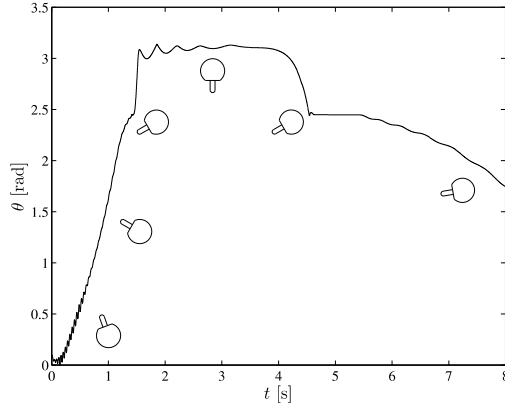


Figure 12. Inclination of the Tippe-Top ($R = 5 \cdot 10^{-4}$ m).

derivatives $\gamma_{Ni} = \dot{g}_{Ni}$ (almost everywhere)

$$\gamma_{Ni} = \dot{z}_S - a_i \dot{\theta} \sin \theta, \quad i = 1, 2$$

or $\gamma_{Ni} = \mathbf{W}_{Ni}^T \dot{\mathbf{q}} + \tilde{w}_{Ni}$. The velocity of point C on the spherical part top is given by $\mathbf{v}_C = \mathbf{v}_S + \boldsymbol{\omega} \times \mathbf{r}_{SC}$ where \mathbf{r}_{SC} is the vector from the center of mass S to the point C , i.e. $\mathbf{r}_{SC} = \mathbf{r}_C - \mathbf{r}_S$. The velocity \mathbf{v}_C in the frame \mathbf{e}^1 becomes

$$\mathbf{v}_C^1 = \begin{bmatrix} \dot{x}_S + (a_1 \dot{\phi} + r_1 \dot{\psi}) \sin \theta \cos \varphi + \dot{\theta} (a_1 \cos \theta - r_1) \sin \varphi \\ \dot{y}_S + (a_1 \dot{\phi} + r_1 \dot{\psi}) \sin \theta \sin \varphi - \dot{\theta} (a_1 \cos \theta - r_1) \cos \varphi \\ \dot{z}_S - a_1 \dot{\theta} \sin \theta \end{bmatrix},$$

where the component in \mathbf{e}_3^1 is zero when $\gamma_{N1} = 0$.

The tangential contact velocity is a vector in the $(\mathbf{e}_1^1, \mathbf{e}_2^1)$ plane. The tangential contact velocity at contact point 1 is given by the components of \mathbf{v}_C^1 in the $(\mathbf{e}_1^1, \mathbf{e}_2^1)$ directions

$$\boldsymbol{\gamma}_{T1} = \begin{bmatrix} \dot{x}_S + (a_1 \dot{\phi} + r_1 \dot{\psi}) \sin \theta \cos \varphi + \dot{\theta} (a_1 \cos \theta - r_1) \sin \varphi \\ \dot{y}_S + (a_1 \dot{\phi} + r_1 \dot{\psi}) \sin \theta \sin \varphi - \dot{\theta} (a_1 \cos \theta - r_1) \cos \varphi \end{bmatrix}.$$

In the same way we can find $\boldsymbol{\gamma}_{T2}$, which we write in the form $\boldsymbol{\gamma}_{Ti} = \mathbf{W}_{Ti}^T \dot{\mathbf{q}} + \tilde{w}_{Ti}$ with $i = 1, 2$.

The relative spin of a contact point is the projection of the Poisson vector on the \mathbf{e}_3^1 axis, i.e. ω_3^1 . The spin velocity vector is the product of spin angular velocity and a contact radius R_i and given by $\gamma_{\tau i} = \omega_3^1 R_i = (\dot{\phi} + \dot{\psi} \cos \theta) R_i = \mathbf{W}_{\tau i}^T \dot{\mathbf{q}} + \tilde{w}_{\tau i}$ for $i = 1, 2$.

Numerical results on the Tippe-Top with an approximated Coulomb-Contensou friction model (tangens hyperbolicus approximation) and a penalty approximation in the normal direction were given in (Friedl, 1997). We will present similar results, but making use of the set-valued Coulomb-Contensou friction

law in tangential direction and Signorini's law in normal direction. We consider for the numerical analysis the same dataset as taken in (Friedl, 1997): $m = 6 \cdot 10^{-3}$ kg, $I_1 = 8 \cdot 10^{-7}$ kgm², $I_3 = 7 \cdot 10^{-7}$ kgm², $g = 9.81$ m/s², $a_1 = 0.3 \cdot 10^{-2}$ m, $a_2 = 1.6 \cdot 10^{-2}$ m, $r_1 = 1.5 \cdot 10^{-2}$ m, $r_2 = 0.5 \cdot 10^{-2}$ m, $\mu_i = 0.3$, $\epsilon_{Ni} = 0$, $R_i = 5 \cdot 10^{-4}$ m for $i = 1, 2$. These parameters are realistic for a wooden commercial Tippe-Top on a wooden floor. A difficult parameter to choose is the contact radius R , which would be according to Hertz law (Johnson, 1985)

$$R_{\text{Hertz}} = \left(\frac{3\rho^* \lambda_N}{4E^*} \right)^{\frac{1}{3}}.$$

We assume that the underground is flat and therefore that $\rho^* = r_1$. The contact force is approximately equal to its stationary value $\lambda_N \approx mg$. Furthermore, we assume the effective modulus of elasticity to be $E^* = 5$ GPa, which is realistic for a wooden toy on a wooden surface. The theoretical radius R_{Hertz} would with these assumptions be about $5 \cdot 10^{-5}$ m, which is much less than the surface roughness of wood ($10^{-4} \dots 10^{-3}$ m). It can therefore be expected that the radius of the contact surface does not follow Hertz' law but depends on the roughness of the contacting bodies. We therefore assume a constant contact radius of $R = 5 \cdot 10^{-4}$ m for both contact points.

The motion of the Tippe-Top was simulated with a four stage Runge-Kutta time-stepping method and with the initial condition (following Friedl (1997)) $z_{S0} = 1.2015 \cdot 10^{-2}$ m, $\theta_0 = 0.1$ rad, $\psi_0 = 180$ rad/s, and all other initial states being equal to zero. The inclination θ during the first 8 seconds of the motion is shown in Figure 12 and the contact distances in Figure 13. The initial condition at $t = 0$ s corresponds to a slightly inclined top which is resting with its body on the floor, i.e. $g_{N1} = 0$ and $g_{N2} > 0$, and is spinning fastly around its axis of revolution. The friction forces in the contact surface cause a frictional torque along the \mathbf{e}_3^1 axis. The frictional torque together with the spin around the \mathbf{e}_3^4 axis causes a gyroscopical torque around nodal axis \mathbf{e}_1^2 which slowly inverts the orientation of the top, $\theta = 0 \rightarrow \theta = \pi$. A high-frequency nutational oscillation is superimposed on the global motion of the top. The stick touches the floor at $t = 1.5$ s, after which the body loses contact with the floor, i.e. $g_{N1} > 0$ and $g_{N2} = 0$. The top turns almost completely upright on the stick during the period $1.6 < t < 4$ s. The rotational speed of the top is gradually reduced due to the dissipation of the friction forces, which causes a re-inversion of the top, $t > 4$ s. The re-inversion causes the body to touch the floor at $t = 4.5$ s. A rocking motion is initiated, which ends in an accumulation point of impacts. The top remains in double-point contact ($g_{N1} = g_{N2} = 0$) during the period $4.6 < t < 5.4$ s. Finally, the contact between stick and floor is opened and the top gradually returns to its trivial non-rotating equilibrium position.

Stationary motion of the Tippe-Top can occur in the trivial

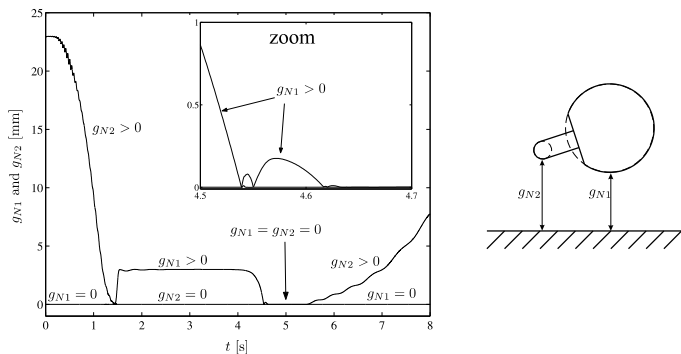


Figure 13. Time-history of the contact distances ($R = 5 \cdot 10^{-4}$ m).

position ($\theta = 0$) with contact between the body and the floor or in an inverted position ($\theta = \pi$) with contact between the stick and the floor. The two equilibria show a similarity and it will therefore prove to be convenient to introduce the following parameters

1. body-floor contact: $a = a_1 > 0$, $r = r_1 > 0$, $r > a$,
2. stick-floor contact: $a = -a_2 < 0$, $r = r_2 > 0$, $r > -a$.

For each case the value of $h = -a + r$, which defines the maximal height of the center of mass S with respect to the floor, is positive $h > 0$. The stability of these equilibria depends on the spin ω and on the geometry of the top. Dissipation will slow down the top and bring it back to rest. The trivial position is therefore in the classical sense always globally asymptotically stable. Still, it is of interest to know whether the top can stay (for some time) on its stick for a certain spin ω and whether the trivial position can become (temporarily) unstable for large values of ω .

The Contensou phenomenon causes the tangential friction force λ_T to be a smooth single-valued function of γ_T for non-zero values of ω (Figure 8). For small values of u , the tangential friction force can be approximated by the smooth relation

$$\lambda_T \approx -\mu\lambda_N \frac{3}{8\pi} \frac{1}{\omega R} \gamma_T = -\varepsilon \gamma_T, \quad (17)$$

with $\varepsilon = \mu mg \frac{3}{8\pi} \frac{1}{\omega R}$. Magnus (1971) presented the necessary and sufficient conditions for local stability of the Tipped-Top in the presence of a smooth friction law using a linear stability analysis. The stability-diagram of the Tipped-Top (Figure 14) shows four regions. Regions II and IV are conditionally stable depending on the critical spin velocity ω_k ,

$$\omega_k^2 = \frac{-amg}{\frac{r}{h} I_1 \left(\frac{I_3}{I_1} - \frac{r}{h} \right)} > 0. \quad (18)$$

A commercial Tipped-Top is designed such that the trivial po-

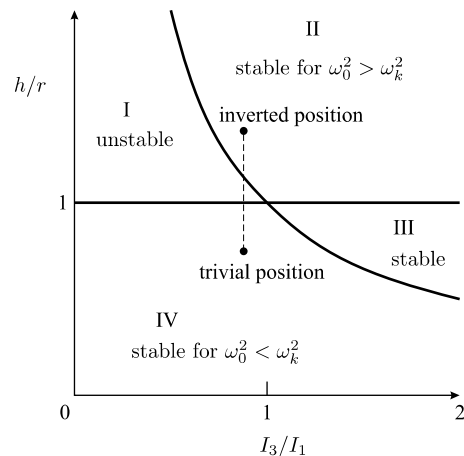


Figure 14. Stability diagram of the Tipped-Top (Magnus, 1971).

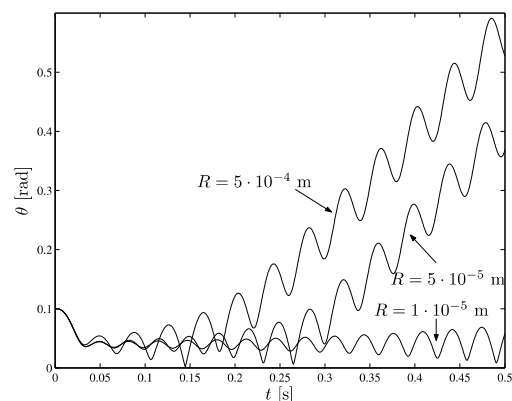


Figure 15. Time-history of the inclination for different contact radii.

sition is located in Region IV, which can become unstable, and the inverted position is located in Region II and can be stable for large values of ω_0 . The stability regions do not depend on ε and do therefore not depend on the contact radius $R > 0$, but the magnitude of the eigenvalues does depend on ε and R .

Figure 15 shows numerical simulations of the Tipped-Top for three values of the contact radius. A smaller contact radius causes a slower inversion of the Tipped-Top, because a decrease of the contact radius also decreases the magnitude of the real part of the eigenvalues. This shows the importance of Coulomb-Contensou's friction law for the dynamics of the system.

CONCLUSION

A set-valued force law for spatial Coulomb-Contensou friction was formulated in this paper within the theory of non-

smooth potentials and is able to describe the smooth nature of the friction forces during slipping/spin as well as the set-valued nature of the friction forces during stick (no slipping, no spin). Other contact and friction effects, such as adhesion and rolling friction, might be described within the same framework.

A higher-order Runge-Kutta time-stepping method was briefly described as an extension to the existing time-stepping method of Moreau. The need for such a higher-order integration method became apparent during the numerical analysis of the Tippe-Top. The Tippe-Top experiences almost no damping and exhibits high-frequency oscillation in the nutation. Numerical simulation with the classical (low-order) time-stepping method yielded fastly diverging solutions, or a fast deadening of the nutational oscillation if integrated with a fully implicit version of the classical time-stepping method. Reducing the step-size led to different results as the divergence or deadening was weakened. The higher-order Runge-Kutta time-stepping method gives the correct result and converges for a reduction of the step-size.

The algebraic inclusion, formed by the equation of motion and the set-valued contact laws, was numerically solved by making use of the Augmented Lagrangian. The (N)LCP formulation of the contact problem, formerly used by the authors, was abandoned as it became fully impractical when applied to Coulomb-Contensou friction. A substantial advantage of the Augmented Lagrangian approach is that it solves the algebraic inclusion for arbitrary admissible sets of contact forces (e.g. the set B_F).

The importance of Coulomb-Contensou friction for the dynamics of mechanical systems was illustrated in this paper by an analysis on the Tippe-Top. Industrial applications with fairly rigid contact between spinning objects, such as ball bearings, grinding devices and drillstrings for oil-wells, motivate research on Coulomb-Contensou friction within a non-smooth formalism.

ACKNOWLEDGMENT

This project was supported by the Royal Dutch Academy of Sciences (KNAW) and the Dutch Technology Foundation (STW).

REFERENCES

- Alart, P. and Curnier, A. (1991). A mixed formulation for frictional contact problems prone to Newton like solution methods. *Computer Methods in Applied Mechanics and Engineering*, 92:353–375.
- Anitescu, M. and Potra, F. A. (1997). Formulating dynamic multi-rigid-body contact problems with friction as solvable linear complementarity problems. *Nonlinear Dynamics*, 14(3):231–247.
- Brogliato, B. (1999). *Nonsmooth Mechanics*. Springer, London, 2 edition.
- Contensou, P. (1963). Couplage entre frottement de glissement et frottement de pivotement dans la théorie de la toupie. In Ziegler, H., editor, *Kreiselp Probleme und Gyrodynamics*, pages 201–216, Berlin. Springer-Verlag. IUTAM Symposium Celedrina 1962.
- Friedl, C. (1997). Der Stehaufkreisel. Master's thesis, Universität Augsburg.
- Glocker, Ch. (1995). *Dynamik von Starrkörpersystemen mit Reibung und Stößen*, volume 18, no. 182 of *Fortschr.-Ber. VDI*. VDI Verlag, Düsseldorf.
- Glocker, Ch. (1998). Formulation of spatial contact situations in rigid multibody systems. *Computer Methods in Applied Mechanics and Engineering*, 177:199–214.
- Glocker, Ch. (2001). *Set-Valued Force Laws, Dynamics of Non-Smooth Systems*, volume 1 of *Lecture Notes in Applied Mechanics*. Springer-Verlag, Berlin.
- Johnson, K. L. (1985). *Contact Mechanics*. Cambridge University Press, Cambridge.
- Leine, R. I., Glocker, Ch., and Van Campen, D. H. (2003). Non-linear dynamics and modeling of some wooden toys with impact and friction. *Journal of Vibration and Control*, 9(1):25–79.
- Magnus, K. (1971). *Kreisel; Theorie und Anwendungen*. Springer-Berlag, Berlin.
- Moreau, J. J. (1988). Unilateral contact and dry friction in finite freedom dynamics. In Moreau, J. J. and Panagiotopoulos, P. D., editors, *Non-Smooth Mechanics and Applications*, volume 302 of *CISM Courses and Lectures*, pages 1–82. Springer, Wien.
- Pfeiffer, F. and Glocker, Ch. (1996). *Multibody dynamics with unilateral contacts*. Wiley, New York.
- Rockafellar, R. T. (1976). Augmented Lagrangians and applications of the proximal point algorithm in convex programming. *Mathematics of Operations Research*, 1(2):97–116.
- Stieglmeier, A. (2001). *Zur numerischen Berechnung strukturvarianter Mehrkörpersysteme*, volume 18, no. 271 of *Fortschr.-Ber. VDI*. VDI Verlag, Düsseldorf.
- Zhuravlev, V. G. (1998). The model of dry friction in the problem of the rolling of rigid bodies. *Journal of Applied Mathematics and Mechanics*, 62(5):705–710.